Journal of Power Sources 222 (2013) 15–20

Contents lists available at SciVerse ScienceDirect

Journal of Power Sources

journal homepage: www.elsevier.com/locate/jpowsour

Investigation of the microstructural effect of Ni–yttria stabilized zirconia anode for solid-oxide fuel cell using micro-beam X-ray absorption spectroscopy analysis

Koichi Hamamoto [a], Toshio Suzuki [a,*], Bo Liang [a], Toshiaki Yamaguchi [a], Hirofumi Sumi [a], Yoshinobu Fujishiro [a], Brian Ingram [b], A. Jeremy Kropf [b], J. David Carter [b]

[a] National Institute of Advanced Industrial Science and Technology (AIST), 2266-98 Anagahora Shimo-shidami, Moriyama-ku, Nagoya 465-0024, Japan
[b] Argonne National Laboratory, Argonne, IL, USA

HIGHLIGHTS

- Micro-beam XAFS Analysis was correlated to electrochemical performance of the cell.
- Ni/NiO fraction at different positions in the anode was shown.
- Oxidation status of Ni in the anode is sensitive to position.

ARTICLE INFO

Article history:
Received 3 April 2012
Received in revised form
6 June 2012
Accepted 31 July 2012
Available online 31 August 2012

Keywords:
Solid-oxide fuel cell
SOFC
Anode
XAS
XANES

ABSTRACT

The microstructural effect of the solid-oxide fuel cell (SOFC) anode on fuel cell performance has been investigated using X-ray absorption spectroscopy (XAS). Anodes were examined after the fuel cell had operated at 600–700 °C using H_2 fuel. The microstructure of micro tubular anodes consisting of conventional Ni–yittria stabilized zirconia (YSZ) has been controlled by altering the co-sintering temperature with the zirconia electrolyte. Impedance analysis has clearly shown that the over-potentials for the gas transport and the electrochemical reactions improve for the anode prepared at lower co-sintering temperatures. Using data from the X-ray absorption near edge structure (XANES) energy region, the metallic Ni fraction as a function of distance from the electrolyte has also been measured for those samples. XANES observation has shown the oxidation status of Ni in the anode is quite sensitive to position relative to the anode/electrolyte interface. These results may be an indication of the positions of the reaction sites for oxide ions and the fuel: assuming the oxidation state of nickel (Ni–O) designates the active triple phase boundary.

1. Introduction

Energy and environmental issues have never been as important world-wide as today. In addition to reducing CO_2 emissions, the efficient use of energy resources is critical. Fuel cells are advantageous in this regard due to their high energy conversion efficiency. Among the variety of fuel cell types, the solid oxide fuel cell (SOFC) has been considered to be ideal as a future power source because it has the highest energy efficiency and potentially the longest operating lifetime [1–5]. Current SOFC research topics focus mainly on lowering the operating temperature below 700 °C, increasing thermal shock resistance for quick start-up, and increasing the redox cycling stability. Such advancements can be achieved by developing new SOFC component materials and improving the electrode microstructures. Many studies related to the electrolyte, anode and cathode materials have been reported [6–11]. In addition to these developments, the influence of electrode microstructure on the cell performance is also revealed [12]; thus, a basic understanding of microstructural effect on the electrode performance becomes more important. For this purpose, X-ray absorption spectroscopy (XAS) was utilized to examine the fractured cross section of micro tubular SOFC anodes to understand the interaction between sintering temperature, operating conditions and the nickel oxidation state.

In this paper, we show the results of microstructural investigation of cells with different anode microstructures, including impedance analysis during fuel cell operation and electron microscopic and X-ray absorption near-edge structure (XANES) micro-spectroscopic analyses on the anodes after the fuel cell operation.

* Corresponding author. Tel.: +81 52 736 7295; fax: +81 52 736 7405.
E-mail address: toshio.suzuki@aist.go.jp (T. Suzuki).

0378-7753/$ – see front matter © 2012 Elsevier B.V. All rights reserved.
http://dx.doi.org/10.1016/j.jpowsour.2012.07.108

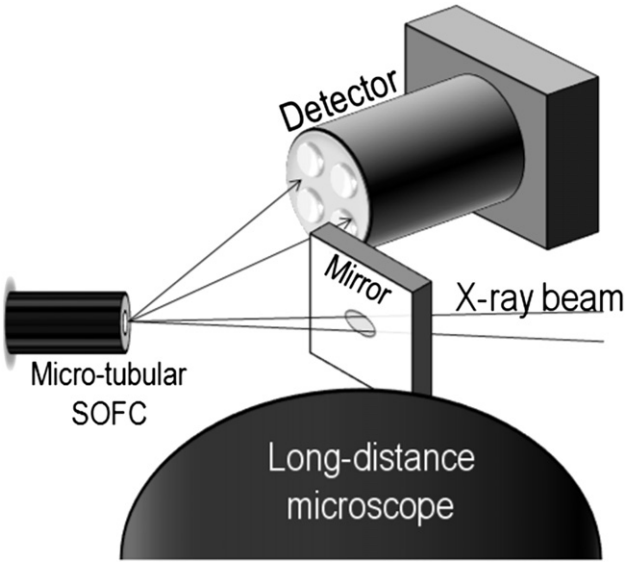

Fig. 1. A perspective drawing of the experiment of Micro-beam X-ray absorption spectroscopy.

2. Experimental

The micro tubular SOFCs reported here consist of nickel-yttria stabilized zirconia (Ni/YSZ) anodes, scandia stabilized zirconia (ScSZ) electrolytes, and $La_{0.6}Sr_{0.4}Co_{0.2}Fe_{0.8}O_3$−x + gadolinia doped ceria (LSCF/GDC) cathodes, with a GDC interlayer between the cathode and the electrolyte. Note that all of the materials used for the SOFC fabrication are commercially available.

2.1. Fabrication

Anode tubes were made from nickel oxide (NiO, Sumitomo Metal Mining Co., Ltd.), 8% yttria stabilized zirconia (YSZ, Tosoh Co., Ltd.), polymethyl methacrylate beads (PMMA, Sekisui Plastics Co., Ltd.), and cellulose (Yuken Kogyo Co., Ltd.). These powders were blended for 1h using a high-viscosity mixer (5DMV-r, Dalton Co., Ltd.); and, after adding the correct amount of water, were kneaded for 30 min under vacuum. The mixture was kept in a closed container over 15 h for aging. Tubes were extruded from the mixture using a metal mold (2.4 mm diameter with 2.0 mm diameter pin) by a piston-type extruder (Ishikawa-Toki Tekko-sho Co., Ltd.).

A slurry for dip-coating the electrolyte was prepared by mixing 10% Sc stabilized zirconia with 1% Ce (ScSZ, Daiichiki-genso Co., Ltd.), solvents (toluene and ethanol), binder (polyvinyl butyral), dispersant (polymer of an amine system) and plasticizer (dioctyl phthalate) for 24 h. The anode tubes were dipped in the slurry and coated at the pulling rate of 1.0 mm s^{-1}. The coated films were dried in air, and co-sintered at 1300 °C (cell A) or 1350 °C (cell B) for 1 h in air. An inter-layer slurry of gadolinia doped ceria (GDC, Shinteu kagaku, Co., Ltd.) was dip-coated on the electrolyte layer of the tube and sintered at 1100 °C. Then, a slurry containing $La_{0.6}Sr_{0.4}Co_{0.2}Fe_{0.8}O_{3-y}$ (LSCF, DOWA Electronics Materials Co., Ltd.) and the GDC with the weight ratio of LSCF:GDC = 7:3 was dip-coated on the inter-layer. The SOFCs were completed by sintering at 1050 °C. The cell size was 1.8 mm diameter and 30 mm length with cathode length of 10 mm, having an effective electrode area of 0.56 cm^2.

2.2. Characterization

The microstructure of the electrodes of the tubular cell was characterized (before and after cell testing) using mercury porosimetry and scanning electron microscopy (SEM) (JEOL, JSM6330F).

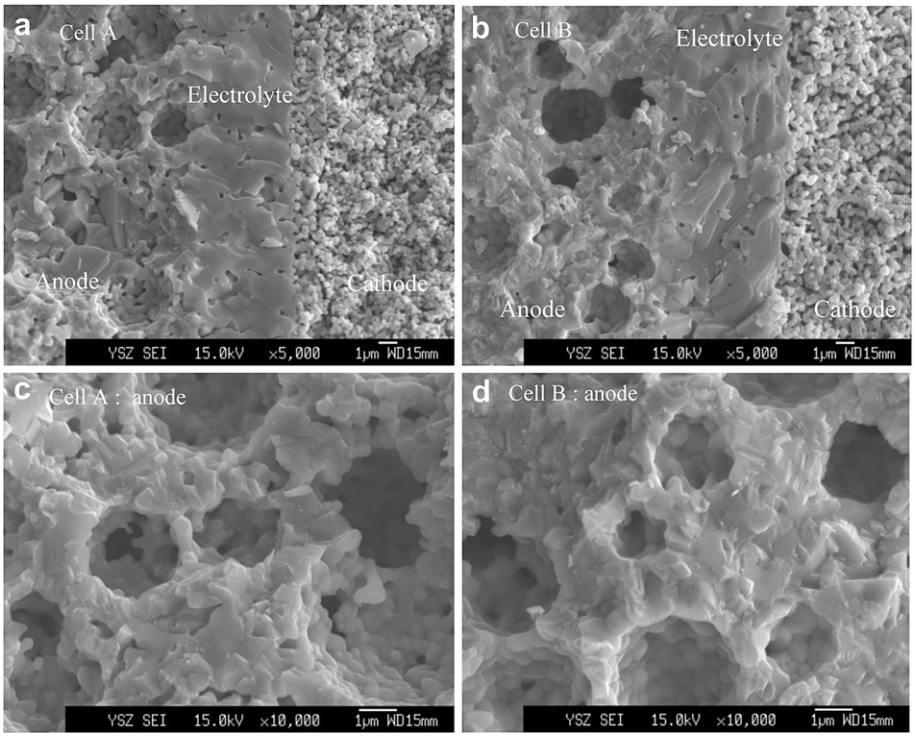

Fig. 2. Cross-sectional fracture SEM images of micro tubular SOFCs prepared with different co-sintering temperatures, (a) Cell A, (b) Cell B, (c) anode of Cell A, and (d) anode of Cell B.

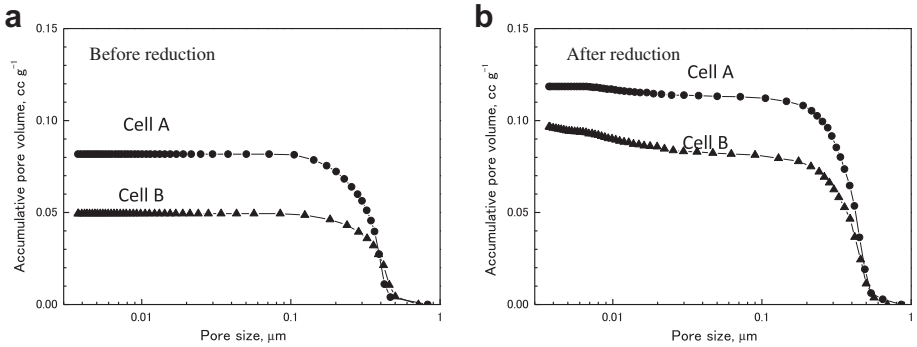

Fig. 3. Pore distribution of the prepared samples A and B (a) before and (b) after the reduction.

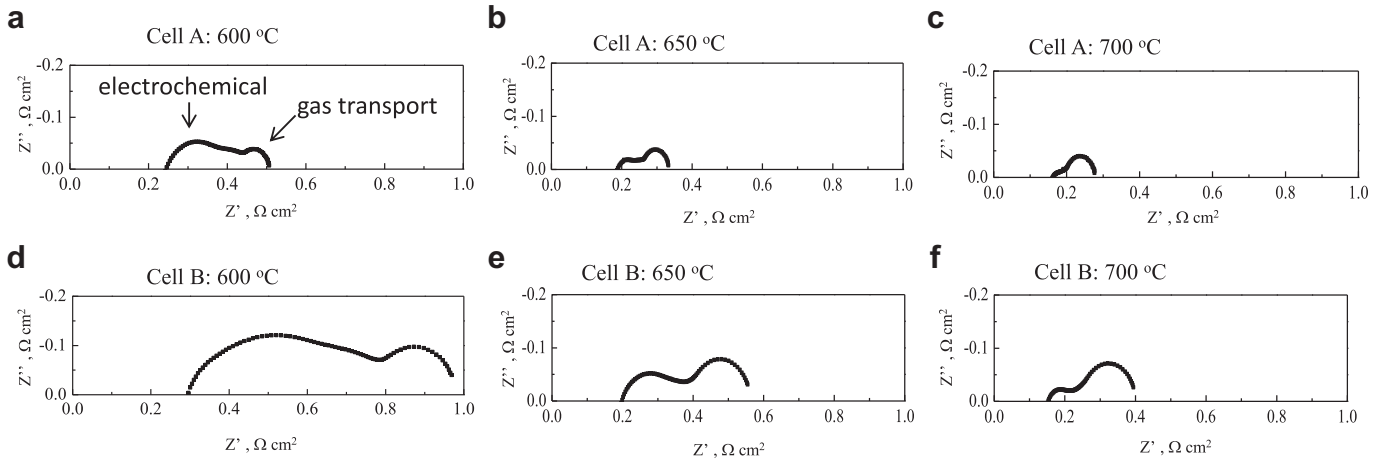

Fig. 4. Impedance spectra of the cells (A and B) obtained at various operating temperatures, Cell A (a) 600 °C (b) 650 °C (c) 700 °C, Cell B (d) 600 °C (e) 650 °C (f) 700 °C.

Cell impedance was investigated at temperatures of 600, 650, 700 °C, respectively; the temperature being monitored by a thermocouple placed near the sample. Silver wire fixed with silver paste was used for current collection for both the anode and cathode. For the anode, current was collected from an edge of the anode tube; and current was collected from the cathode by winding wire around the whole cathode area. Detailed information for experimental setup can be found in previous literature [13]. Diluted hydrogen (20% H_2 in Ar) flowed inside the tubular cell at rates of 54 mL min^{-1} (H_2 flow rate: 16.8 mL min^{-1} per cm^2 of electrode area). Air was supplied to the cathode side at a flow rate of 100 mL min^{-1}. After the measurement, the furnace was turned off and cooled down. Fuel was supplied to the cell until the furnace temperature decreased below 200 °C to avoid cell re-oxidation.

2.3. XAS analysis

The anodes of Cell A and B after testing in the fuel cell conditions were fractured to expose a fresh cross section and examined using Micro-beam XAS in air at room temperature. Micro-beam XAS studies were performed at the Materials Research Collaborative Access Team (MR-CAT) beamline 10-ID at the Advanced Photon Source, Argonne National Laboratory (USA). Fig. 1 shows a perspective drawing of the Micro-beam X-ray Absorption Spectroscopy experiment. A cryogenically cooled Si(111) monochromator selected the incident energy and a rhodium-coated mirror rejected higher order harmonics of the fundamental beam energy. The beam was focused to about a 2 μm × 2 μm spot using a platinum-coated KB mirror pair. All mirror angles were set with a critical energy near 10 keV so that higher order harmonics were attenuated by three reflections. The samples were positioned with the tube ends facing the beam with normal incidence to minimize the beam interaction with multiple layers in the tube. A four-element silicon detector (Vortex ME4, SII NanoTechnology USA Inc.) was used to detect the X-ray fluorescence. This detector was pointed toward the sample at an angle of about 40° from perpendicular. This orientation resulted in a large self-absorption attenuation of the XAS amplitudes, especially for the highly-concentrated metallic nickel layer. The data was processed using Athena [14]. The sample data was aligned using a Ni transmission standard placed to intercept elastically scattered x-rays from a kapton film. A self-absorption correction was made empirically with the "Fluo" algorithm in Athena [14] using the chemical formula: (Ni)46(ZrO2)52(Y2O3)4, angle in: 10° and angle out: 80° for the concentrated metallic nickel regions; and required different angles in: 20° and out: 15° for high NiO concentrated regions to obtain a good fit between the Ni and NiO standards. The relative concentrations of Ni and NiO in each sample were measured using a linear combination fitting algorithm with a fitting range of −20 and 30 eV below and above the edge using transmission metallic Ni and NiO standards.

Table 1
The porosity of the anodes for Cell A and Cell B before and after reduction.

	Anode porosity	
	Before reduction	After reduction
Cell A	34.6%	39.2%
Cell B	22.0%	33.3%

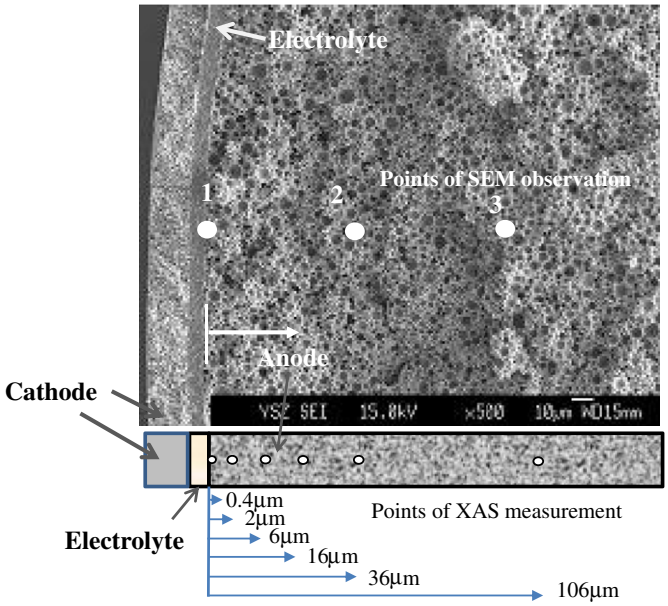

Fig. 5. Positions of SEM observation and XAS analysis.

3. Results and discussion

Fig. 2(a) and (b) shows cross-sectional fracture SEM images of micro tubular SOFCs, Cell A and Cell B, of which the anode tubes were sintered at 1300 and 1350 °C, respectively. All other fabrication processes were identical. The final thickness of the electrolytes is ~6 μm and the cathode microstructure of the two cells is comparable. However, the microstructure of the anode is shown to be quite different as shown in Fig. 2(c) and (d). The constituent particle size of the anode in Cell A (0.3 ~ 0.4 μm) is shown to be smaller and more distinct than that of Cell B (0.5 ~ 0.6 μm) due to the lower sintering temperature. The cumulative pore-volume distribution (measured by mercury porosimetry) of the anodes for cell A and B before reduction (oxide state) and after reduction are shown in Fig. 3(a) and (b). The dominant pore sizes of the anodes before reduction are 0.1–0.3 μm, as shown in Fig. 3(a) After reduction, the distribution shifts to larger pore diameter and volume, due to the reduction from NiO to Ni, as shown in Fig. 3(b). The pore volume of Cell A increases from 0.08 to 0.12 $cm^3\ g^{-1}$, whereas the pore volume of Cell B increases from 0.05 to 0.09 $cm^3\ g^{-1}$. The final pore volume of Cell A is 33% greater than Cell B due to the initial sintering conditions. It is noteworthy that the formation of meso-pores in the range of 10 nm can also be identified in both cells: although, more prominent in Cell B than in Cell A.

Table 1 summarizes the porosity of the anodes before and after reduction. Cell A showed a small increase (13%) of the porosity after reduction from 34.6 to 39.2%, probably due to the original microstructure included sufficient pores and smaller NiO particles which lead to a smaller increment of porosity after reduction. The porosity of Cell B increased by 50% from 22 to 33% porosity.

Fig. 4 shows the impedance spectra, obtained at OCV, of cells A and B at cell temperatures: 600, 650 and 700 °C. As can be seen, at least two semi-circles are observed for all spectra, namely high frequency (left hand side) and low frequency (right hand side)

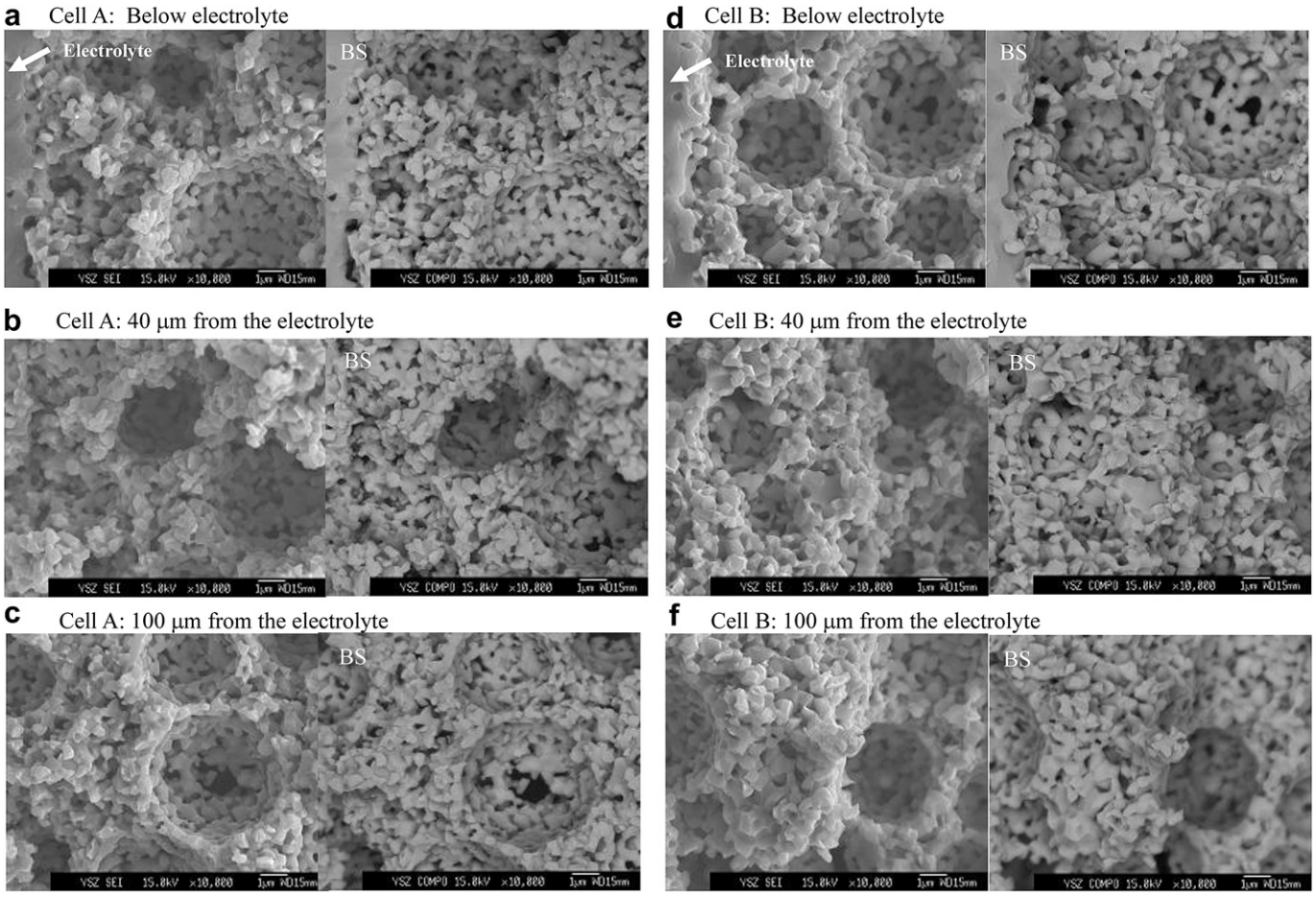

Fig. 6. Fracture SEM images of the anode microstructures after fuel cell test (Cell A and B) at each position with the back scattering (BS) images obtained at the same position.

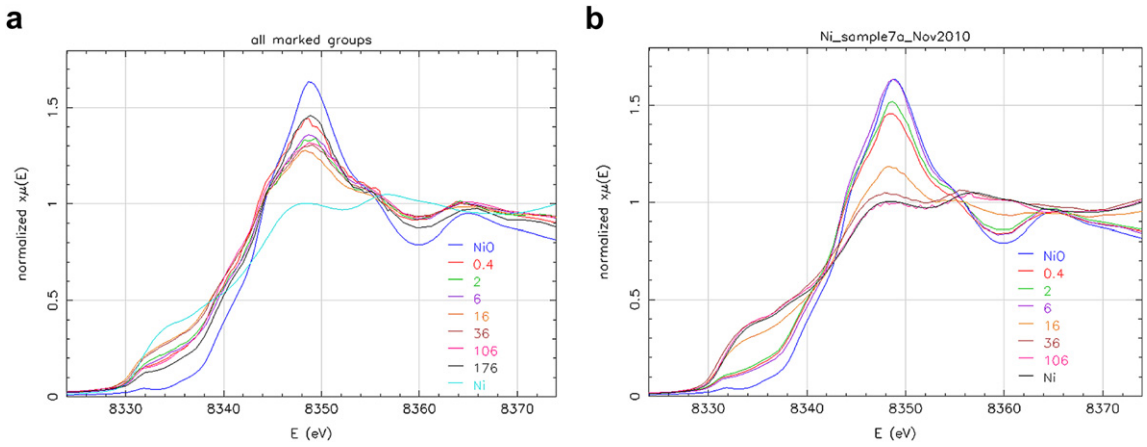

Fig. 7. XANES spectra of the anode (corrected for self-absorption) obtained at each position for (a) cell A and (b) cell B after the fuel cell test. Curves of Ni and NiO were obtained using standard specimen. Numerals in the graphs correspond to the distance from the electrolyte indicated in Fig. 5.

semi-circles. Each semi-circle is typically assigned as electrochemical process and gas transport overpotential, respectively. Overall, the high frequency semi-circle of cell A is also much smaller than that of cell B, showing improved catalytic activity as well as gas transport overpotential. The cell performance corresponds to the grain structure in Fig. 2, and pore data in Fig. 3 and Table 1; where Cell A has smaller grains, and a larger cumulative pore volume and porosity for improved gas transport. These results are comparable to previous reports for our Ni–ScSZ anode [12].

Fig. 5 shows the position of SEM and XAS analysis for the cell A and B after fuel cell test. The SEM images shown in Fig. 5 were taken (1) in the vicinity of the electrolyte, (2) at 40 μm and (3) at 100 μm from the electrolyte interface. XAS data was collected at 0.4, 2, 6, 16, 36 and 106 μm distances from the electrolyte interface.

Fig. 6(a)–(f) shows the SEM images of cells A and B obtained at the positions shown in Fig. 5. "BS" in Fig. 6 stands for "Back Scattering" and the BS images were obtained at the exact position of the SEM images. Smaller particles of Ni were observed for cell A compared to cell B. At a glance, however, there is not much difference in the microstructure of each position. On the contrary, XAS observation showed distinguishable chemical differences between cell A and cell B. Fig. 7 shows XANES spectra of the anodes (corrected for self-absorption) obtained at each position for cell A and cell B after the fuel cell test. Curves of Ni and NiO in Fig. 7 were obtained using standard specimen. Numerals in the graphs correspond to the distance from the electrolyte indicated in Fig. 5. In Fig. 7(a): Cell A, the Ni K-edge data resembles the NiO standard, especially at positions closer to the electrolyte. On the other hand, in Fig. 7(b): Cell B showed that Ni was oxidized up to 36 μm from the electrolyte and then became more metallic nearer to the surface of the anode facing the reducing atmosphere. Assuming that the oxidation state of Ni (Ni–O) being possible triple phase boundary, the results of cell A in Fig. 7(a) indicated that the anode of cell A had large number of possible reaction points, which positively influence to the cell performance. The impedance analysis in Fig. 3 also showed large reduction of high frequency semi-circle for cell A compared to cell B, which may support the XAS results in Fig. 7.

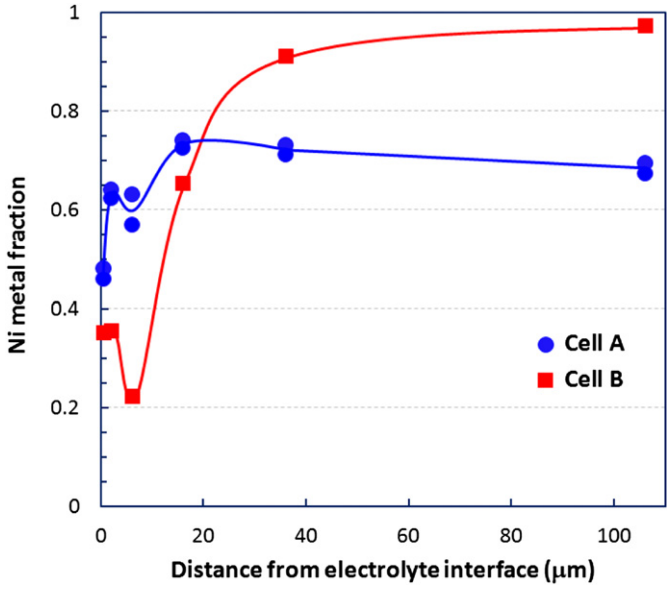

Fig. 8. Ni metal fraction (Ni/Ni + NiO) as a function of distance from the electrolyte.

Using the results in Fig. 7, Ni metal fraction (Ni/Ni + NiO) as a function of distance from the electrolyte was estimated for Cell A and Cell B. As can be seen in Fig. 8, while Cell B confined the low Ni fraction range around 20 μm from the electrolyte, Cell A showed wide range of NiO distribution in the anode. This can be attributed to high porosity as well as smaller Ni particles which resulted in enhancing the anode performance. It was also worth noting that the Ni fraction can be as low as 20% at the vicinity of the electrolyte for Cell B.

Further XAS investigation of the anode including EXAFS region is necessary in order to gain the understanding and correct interpretation of the data, however, the results indicated that XAS study has a potential to understand the electrochemical mechanism in SOFC anode and considered to be excellent tool for further development of SOFC toward the commercialization.

4. Conclusions

The microstructural effect of solid-oxide fuel cell anode on the fuel cell performance was investigated using electrochemical impedance analysis and XAS analysis. The microstructure of the anode consisting of conventional Ni–yittria stabilized zirconia (YSZ) was controlled by the co-sintering temperature with the electrolyte. Impedance analysis clearly showed that the overpotentials for the gas transport and the electrochemical reactions improve for the anode prepared at lower co-sintering temperatures. XAS observation has shown the oxidation status of Ni in the

anode sensitively, which may indicate the reaction sites (triple phase boundary) for oxide ions and the fuel. Further investigation is necessary for better understanding of the phenomena.

Acknowledgments

This work is supported by Minister of Economy, Trade and Industry, Japan–U.S. cooperation project for research and standardization of Clean Energy Technologies. MRCAT operations are supported by the Department of Energy and the MRCAT member institutions.

References

[1] N.Q. Minh, J. Am. Cer. Soc. 78 (1993) 563–588.
[2] O. Yamamoto, Electrochim. Acta 45 (2000) 2423–2435.
[3] S.C. Singhal, Solid State Ionics 152–153 (2002) 405–410.
[4] B.C.H. Steele, A. Heinzel, Nature 414 (2001) 345–352.
[5] H. Yokokawa, N. Sakai, T. Horita, K. Yamaji, M.E. Brito, MRS Bull. 30 (2005) 591–595.
[6] J.W. Yan, H. Matsumoto, M. Enoki, T. Ishihara, Electrochem. Solid-State Lett. 8 (2005) A389–A391.
[7] Z.P. Shao, S.M. Haile, Nature 431 (2004) 170–173.
[8] S.W. Tao, J.T.S. Irvine, Nat. Mater. 2 (2003) 320–323.
[9] K. Eguchi, T. Setoguchi, T. Inoue, H. Arai, Solid State Ionics 52 (1992) 165–172.
[10] T. Hibino, A. Hashimoto, K. Asano, M. Yano, M. Suzuki, M. Sano, Electrochem. Solid-State Lett. 5 (2002) A242–A244.
[11] E.D. Wachsman, Solid State Ionics 152 (2002) 657–662.
[12] T. Suzuki, M.H. Zahir, Y. Funahashi, T. Yamaguchi, Y. Fujishiro, M. Awano, Science 325 (2009) 852–855.
[13] T. Suzuki, T. Yamaguchi, Y. Fujishiro, M. Awano, J. Electrochem. Soc. 153 (2006) A925–A928.
[14] B. Ravel, Athena 0.8.054. Available from: http://cars9.uchicago.edu/ifeffit/Downloads, 2008 (accessed 18.05.11).